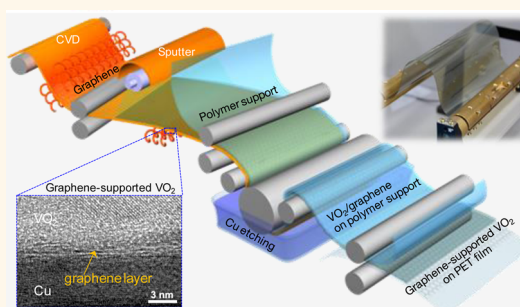


# Flexible Thermochromic Window Based on Hybridized VO<sub>2</sub>/Graphene

Hyeongkeun Kim,<sup>†,▽</sup> Yena Kim,<sup>†,\*,▽</sup> Keun Soo Kim,<sup>§,▽</sup> Hu Young Jeong,<sup>⊥</sup> A-Rang Jang,<sup>||</sup> Seung Ho Han,<sup>†</sup> Dae Ho Yoon,<sup>\*</sup> Kwang S. Suh,<sup>||</sup> Hyeon Suk Shin,<sup>||</sup> TaeYoung Kim,<sup>†,\*,#,\*</sup> and Woo Seok Yang<sup>†,\*</sup>

<sup>†</sup>Electronic Materials and Device Research Center, Korea Electronics Technology Institute, Gyeonggi-do 463-816, Korea, <sup>‡</sup>School of Advanced Materials Science and Engineering, Sungkyunkwan University, Suwon 440-746, Korea, <sup>§</sup>Department of Physics and Graphene Research Institute, Sejong University, Seoul 143-747, Korea, <sup>⊥</sup>UNIST Central Research Facilities and School of Mechanical & Advanced Materials Engineering and <sup>||</sup>Interdisciplinary School of Green Energy, Low Dimensional Carbon Materials Center, and KIER-UNIST Advanced Center for Energy, Ulsan National Institute of Science and Technology (UNIST), Ulsan 689-798, Korea, <sup>\*</sup>Department of Materials Science and Engineering, Korea University, Seoul 136-701, Korea, and <sup>#</sup>Department of Mechanical Engineering and the Materials Science and Engineering Program, The University of Texas at Austin, Austin, Texas 78712, United States. <sup>▽</sup>These authors contributed equally to this work.

**ABSTRACT** Large-scale integration of vanadium dioxide (VO<sub>2</sub>) on mechanically flexible substrates is critical to the realization of flexible smart window films that can respond to environmental temperatures to modulate light transmittance. Until now, the formation of highly crystalline and stoichiometric VO<sub>2</sub> on flexible substrate has not been demonstrated due to the high-temperature condition for VO<sub>2</sub> growth. Here, we demonstrate a VO<sub>2</sub>-based thermochromic film with unprecedented mechanical flexibility by employing graphene as a versatile platform for VO<sub>2</sub>. The graphene effectively functions as an atomically thin, flexible, yet robust support which enables the formation of stoichiometric VO<sub>2</sub> crystals with temperature-driven phase transition characteristics. The graphene-supported VO<sub>2</sub> was capable of being transferred to a plastic substrate, forming a new type of flexible thermochromic film. The flexible VO<sub>2</sub> films were then integrated into the mock-up house, exhibiting its efficient operation to reduce the in-house temperature under infrared irradiation. These results provide important progress for the fabrication of flexible thermochromic films for energy-saving windows.



**KEYWORDS:** smart windows · vanadium dioxide · graphene · flexible thermochromic window · roll transfer

With growing demands for energy-saving technologies, vanadium dioxide (VO<sub>2</sub>) is considered to be a promising candidate for energy-efficient smart windows.<sup>1</sup> VO<sub>2</sub> undergoes a fully reversible metal–insulator transition (MIT) at a temperature of 68 °C, coupled with a structural phase transition between monoclinic VO<sub>2</sub>(M) phase and rutile VO<sub>2</sub>(R) phase.<sup>2–5</sup> The first-order phase transition in VO<sub>2</sub> is accompanied by a dramatic modification of the conductivity on several orders of magnitude and the corresponding optical transmittance; that is, the low-temperature insulating VO<sub>2</sub>(M) is infrared-transparent, while the high-temperature metallic VO<sub>2</sub>(R) is opaque in the infrared region. These unique features of VO<sub>2</sub> have sparked numerous potential applications in field-effect transistors, switches, sensors, and thermochromic coatings.<sup>1,6–10</sup>

The VO<sub>2</sub> phase with favorable transition characteristics has been synthesized by the techniques capable of precisely controlling

oxygen partial pressure such as sputtering deposition,<sup>10</sup> pulsed laser deposition,<sup>11</sup> ion implantation,<sup>12</sup> and chemical vapor deposition (CVD),<sup>13</sup> which typically requires high-temperature processing. While the integration of VO<sub>2</sub> on mechanically flexible substrates is potentially promising for the realization of flexible thermochromic films as next-generation smart windows, high-temperature conditions required to form VO<sub>2</sub> limit the choice of substrates to rigid ones such as glass and sapphire.<sup>14</sup>

Toward the fabrication of flexible VO<sub>2</sub> films, several approaches may be taken into consideration. One is to grow VO<sub>2</sub> directly on flexible substrates, though it is technically hampered due to the lack of low-temperature VO<sub>2</sub> synthetic methods. In this sense, solution-based synthesis of VO<sub>2</sub> and its deposition on flexible substrate at low temperature may be a good option for the low-cost and large-area fabrication.<sup>15–21</sup> However, flexible thermochromic films with

\* Address correspondence to taeykim@utexas.edu, wsyang@keti.re.kr.

Received for review January 23, 2013 and accepted June 11, 2013.

Published online June 11, 2013  
10.1021/nn400358x

© 2013 American Chemical Society

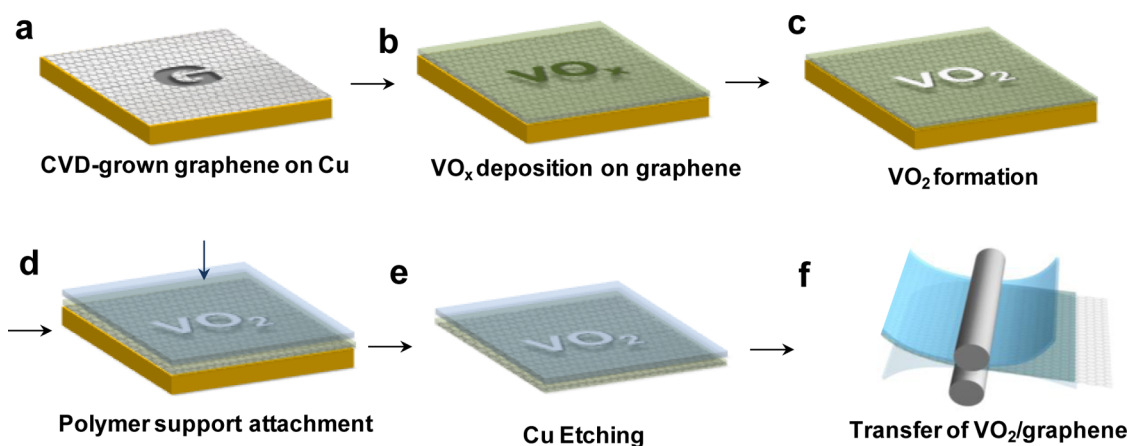


**Figure 1.** Schematic of the fabrication of graphene-supported flexible VO<sub>2</sub> film. (a) Synthesis of graphene on a Cu foil using the chemical vapor deposition (CVD) method. (b) VO<sub>x</sub> deposition on graphene by RF sputtering. (c) Postannealing for VO<sub>2</sub> formation. (d) Lamination of VO<sub>2</sub>/graphene/Cu with thermal release tape etching of underlying Cu foil. (e) Transfer of VO<sub>2</sub>/graphene onto a flexible substrate.

VO<sub>2</sub> particulates prepared through solution-based synthesis often suffer from their modest quality or durability with the metal–insulator phase being often smeared out.<sup>17–21</sup>

Another option is to synthesize highly crystalline VO<sub>2</sub> on the rigid substrates using conventional high-temperature methods and transfer it onto flexible substrates, which may provide a new pathway to fabricate VO<sub>2</sub>-based thermochromic films on flexible substrates. Here, our approach is based on the utilization of graphene as an atomically thin two-dimensional support for VO<sub>2</sub>. With key advantages such as high optical transmission, thermal stability, and mechanical flexibility,<sup>16,22–24</sup> graphene may be an ideal support for the formation of high-quality VO<sub>2</sub>. We further demonstrate that graphene-supported VO<sub>2</sub> films can be easily transferred to flexible substrates, taking advantage of well-established graphene transfer techniques.<sup>25,26</sup> The fabricated VO<sub>2</sub>-based film is mechanically flexible, while maintaining a fully reversible phase transition feature with good optical switching efficiencies. To our knowledge, this is the first demonstration of a method that allows for the deposition of VO<sub>2</sub> on a plastic substrate, thereby producing a flexible VO<sub>2</sub>-based thermochromic film.

## RESULTS AND DISCUSSION

The procedure for the preparation of flexible VO<sub>2</sub>-based thermochromic film is outlined in Figure 1. In the first step, we grew single- or few-layer graphene on copper (Cu) foils by the CVD method (Supporting Information, Figure S1)<sup>25–27</sup> and used them (graphene/Cu) as a support for VO<sub>x</sub> crystals. Amorphous and substoichiometric VO<sub>x</sub> (~40 nm thick) was deposited onto graphene by RF magnetron sputtering of vanadium metal. Following the VO<sub>x</sub> deposition, a VO<sub>x</sub>/graphene/Cu was then annealed at 500 °C with O<sub>2</sub> flow of 50 sccm to render the film crystalline and

near-stoichiometric VO<sub>2</sub> (Supporting Information, Figure S1). As-produced graphene-supported VO<sub>2</sub> on Cu foil (VO<sub>2</sub>/graphene/Cu) was then attached to a thermal release tape and floated on 0.1 M of ammonium persulfate solution to etch Cu foils. After several washes with deionized water, graphene-supported VO<sub>2</sub> (VO<sub>2</sub>/graphene) on thermal release tape was laminated with poly(ethyleneterephthalate) (PET) film using rollers and exposed to mild heat (120 °C), through which the VO<sub>2</sub>/graphene was transferred to PET film (Supporting Information, Figure S2).<sup>25</sup> An alternative transfer process with the use of polymer backing film (*e.g.*, poly(methylmethacrylate), PMMA) was also possible as follows: VO<sub>2</sub>/graphene/Cu was coated with a thin film of PMMA; the underlying Cu was etched; VO<sub>2</sub>/graphene was transferred to either flexible or rigid substrates.<sup>25–27</sup> Our approach to use graphene as a support for VO<sub>2</sub> growth and a transferring medium allows for the fabrication of large-area (up to ~8 in.) and flexible graphene-supported VO<sub>2</sub> film (VO<sub>2</sub>/graphene/PET), as shown in Supporting Information Figure S2. We note that, in a control experiment where VO<sub>2</sub> is directly deposited on graphene-free Cu foil (VO<sub>2</sub>/Cu), transfer of VO<sub>2</sub> to PET substrates was unsuccessful (Supporting Information, Figure S2), which is an indication that graphene is a key element to transfer VO<sub>2</sub> to the PET substrate.

The morphology and structure of VO<sub>2</sub> crystals on both graphene support and graphene-free Cu substrate were examined using high-resolution transmission electron microscopy (TEM) (Figure 2). Cross-sectional TEM image of graphene-free VO<sub>x</sub> on Cu substrate (VO<sub>x</sub>/Cu) (Figure 2a) revealed that polycrystalline VO<sub>x</sub> nanostructures with sizes ~100 nm are rather loosely distributed as islands on the Cu substrate. These sparsely distributed VO<sub>x</sub> islands on the Cu substrate were difficult to transfer to PET substrates as described earlier, presumably due to loosely bound VO<sub>x</sub> island morphology. The fast Fourier transform

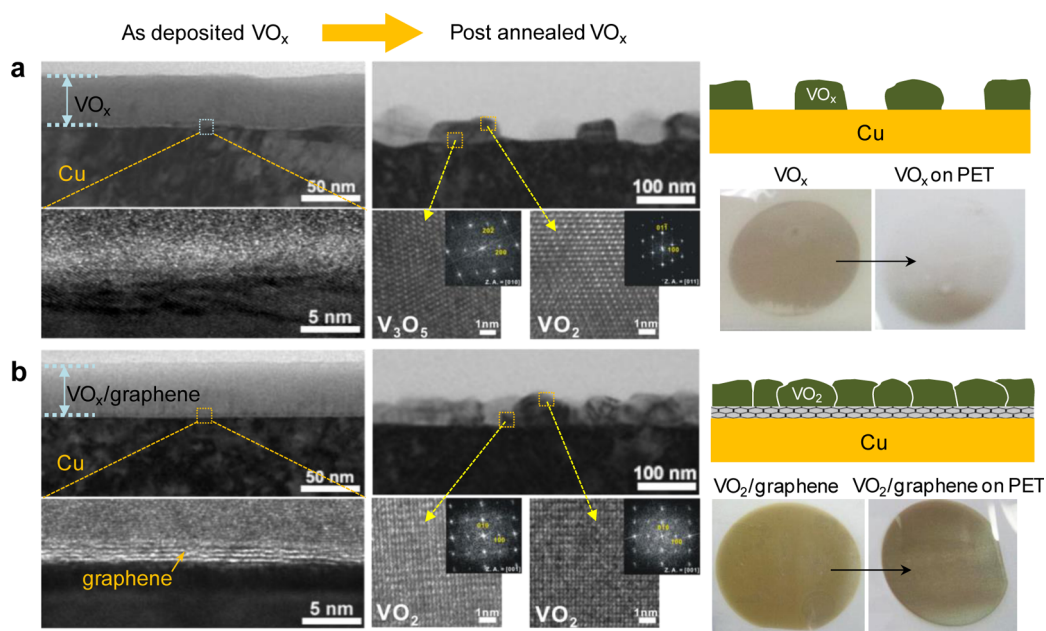


**Figure 2.** Structural characterization of the graphene-supported  $\text{VO}_2$ . (a) High-resolution transmission electron microscopy (HR-TEM) of the cross section of as-deposited and postannealed  $\text{VO}_x$  on graphene-free copper substrate ( $\text{VO}_x/\text{Cu}$ ). The postannealing of graphene-free  $\text{VO}_x$  led to the formation of sparsely distributed  $\text{VO}_x$  crystals. (b) HR-TEM of the cross section of as-deposited and postannealed graphene-supported  $\text{VO}_2$  on copper ( $\text{VO}_2/\text{graphene}/\text{Cu}$ ). The postannealing of graphene-supported  $\text{VO}_x$  afforded the formation of densely interlinked  $\text{VO}_2$  crystals. The FFT patterns after postannealing were indexed to an identical  $\text{VO}_2$  crystalline phase. Photographs show  $\text{VO}_2/\text{graphene}$  laminated with thermal release tape (left) and  $\text{VO}_2/\text{graphene}$  transferred to PET film (right).

(FFT) patterns were taken from two different spots (top and bottom region) to investigate the crystal structure of the graphene-free  $\text{VO}_x$  island along the thickness direction. FFT analysis shows that the crystalline phase of  $\text{VO}_x$  in these two spots can be indexed to  $\text{VO}_2$  and  $\text{V}_3\text{O}_5$ , indicating a mixture of vanadium oxides with a different oxidation state. In contrast, imaging of the cross sections of graphene-supported  $\text{VO}_2$  on Cu ( $\text{VO}_2/\text{graphene}/\text{Cu}$ ) shows contiguously interlinked  $\text{VO}_2$  nanocrystals on graphene support (Figure 2b).<sup>28</sup> In the magnified TEM image of the  $\text{VO}_2/\text{graphene}/\text{Cu}$  sample, the graphene of single to triple layers is also clearly visible between the  $\text{VO}_2$  and Cu layer, with the average interlayer spacing of  $\sim 0.34$  nm (Supporting Information, Figure S3). The FFT patterns taken from two randomly selected spots indicate a coherent crystalline structure of graphene-supported  $\text{VO}_2$  which is indexed to the  $\text{VO}_2(\text{M})$ . Although further structural and chemical analysis of graphene-supported  $\text{VO}_2$  crystals with X-ray diffraction (XRD) and X-ray photoelectron spectroscopy (XPS) showed that it is not composed of pure  $\text{VO}_2$  crystals and rather contains a trace amount of other  $\text{VO}_x$  compounds with different oxidation state (Supporting Information, Figures S4 and S6); this result along with other analysis data suggests that the  $\text{VO}_2$  phase was dominantly formed on graphene support. In addition, it is evident that graphene serves to aid the formation of densely interlinked  $\text{VO}_2$  nanocrystals and therefore permits the straightforward transfer of  $\text{VO}_2$  to PET film.

For further characterization, the structures of  $\text{VO}_2$  and graphene were determined from Raman spectroscopy

(Figure 3). In contrast to the graphene-free  $\text{VO}_x$  sample (Figure 3a, black line), the graphene-supported  $\text{VO}_2$  (transferred to  $\text{SiO}_2/\text{Si}$  substrate,  $\text{VO}_2/\text{graphene}/\text{SiO}_2$ ) (Figure 3a, red line) shows a typical Raman feature of CVD-grown graphene:  $I_G/I_{2D}$  of 0.62 and a symmetric 2D band centered at  $\sim 2694$   $\text{cm}^{-1}$  with full width at half-maximum (fwhm) of  $\sim 38$   $\text{cm}^{-1}$ .<sup>25,26</sup> We note that there is a slight increase in the D-peak ( $1350$   $\text{cm}^{-1}$ ) intensity of graphene after  $\text{VO}_2$  formation, whereas the as-synthesized graphene shows a minimal D-peak indicating a negligibly small portion of structural defects (Supporting Information, Figure S5).<sup>25</sup> The increase in D-peak was attributed to high-temperature oxidation of graphene during postannealing of  $\text{VO}_x$  at  $500$   $^\circ\text{C}$  under  $\text{O}_2$  flowing (Supporting Information, Figure S5)<sup>28–30</sup> (see Supporting Information for further Raman analysis).

The Raman features for  $\text{VO}_2$  were displayed in Figure 3b. Both graphene-free ( $\text{VO}_x/\text{Cu}$ ) and graphene-supported  $\text{VO}_2$  ( $\text{VO}_2/\text{graphene}/\text{Cu}$ ) show several peaks ( $144, 194, 226, 262, 310, 342, 389, 445, 500,$  and  $615$   $\text{cm}^{-1}$ ) corresponding to the characteristic vibration modes assigned to monoclinic  $\text{VO}_2$ .<sup>31</sup> However, the Raman peaks of  $\text{VO}_2/\text{graphene}/\text{Cu}$  are more pronounced as compared with those of  $\text{VO}_x/\text{Cu}$ . This is likely due to the intensified Raman signals originating from the dense  $\text{VO}_2$  distribution on the graphene support.

To gain more insights into the structural phase transition of graphene-supported  $\text{VO}_2$  film, the evolution of Raman peaks was monitored as a function of temperature (Figure 3c). With increasing temperature,

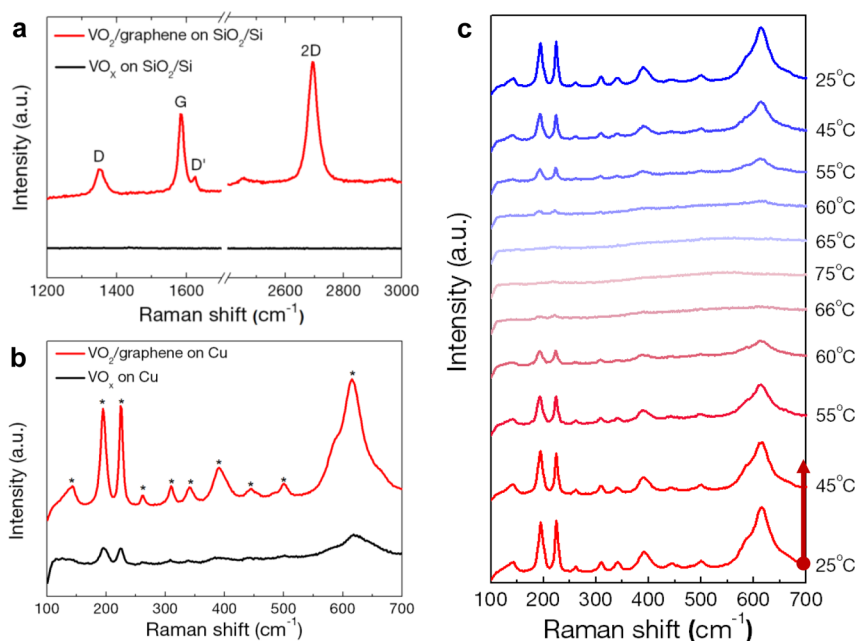


**Figure 3.** Raman spectral analysis of the graphene-supported VO<sub>2</sub>. (a,b) Raman spectra (excited by 532 nm laser) of graphene-supported VO<sub>2</sub> in comparison with graphene-free VO<sub>x</sub>. (c) Sequential Raman spectra of graphene-supported VO<sub>2</sub> on heating and cooling cycle.

the characteristic Raman peaks of monoclinic VO<sub>2</sub> diminish through intermediate phase coexistence regimes and then completely disappear at  $\sim 70$  °C, indicating a structural transition of low-temperature VO<sub>2</sub>(M) into the high-temperature VO<sub>2</sub>(R) phase.<sup>30,32</sup> With decreasing temperature, the monoclinic signature reappears, showing the reverse transition from VO<sub>2</sub>(R) to VO<sub>2</sub>(M) phase. Therefore, the graphene-supported VO<sub>2</sub> displays the prototypical signatures of a reversible first-order transition.

The chemical compositions of VO<sub>2</sub> were probed by X-ray photoelectron spectroscopy (XPS) (Figure 4). The XPS core-level spectra of V2p<sub>3/2</sub> and O1s for the graphene-supported and graphene-free VO<sub>x</sub> on copper are shown in Figure 4a. For the graphene-supported VO<sub>2</sub> on copper (VO<sub>2</sub>/graphene/Cu), the V2p<sub>3/2</sub> spectrum displays a peak with a maximum at 516.6 eV that can be attributed to a 4+ oxidation state of vanadium.<sup>33</sup> However, the V2p<sub>3/2</sub> spectrum of the graphene-free VO<sub>x</sub> (VO<sub>x</sub>/Cu) differs in shift to lower binding energy, indicating that V<sup>+5</sup> is the primary oxidation state. The measurement of depth-dependent O/V ratio also shows that the stoichiometry for graphene-supported VO<sub>2</sub> is nearly uniform across the VO<sub>2</sub> film thickness, whereas nonstoichiometry was observed for VO<sub>x</sub>/Cu sample (Figure 4b). These results indicate that VO<sub>x</sub> film directly grown on Cu has a formula significantly deviating from VO<sub>2</sub>, which is consistent with the result from TEM and XRD measurement. In addition, graphene-free VO<sub>x</sub> shows a significant amount of Cu contaminants which likely migrate from the Cu foil into the VO<sub>x</sub> layer during a high-temperature annealing process, while graphene-supported VO<sub>2</sub> shows a negligible level of Cu contents in the VO<sub>2</sub> layer. This result indicates

that graphene serves as a diffusion barrier providing a physical separation between the Cu and VO<sub>x</sub> layers.<sup>34</sup>

In addition, the graphene layer plays a role in suppressing oxidation of the Cu layer as evidenced by the comparison of Cu2p XPS spectra (Figure 4c). The XPS spectra of Cu foils show two main Cu peaks at binding energies of 932.3 and 952.3 eV corresponding to Cu2p<sub>3/2</sub> and Cu2p<sub>1/2</sub>, respectively.<sup>34</sup> However, the VO<sub>x</sub>/Cu sample shows multiple Cu peaks that can be assigned to different copper oxides, such as Cu<sub>2</sub>O (932.5 and 952.1 eV), CuO (934.3 and 953.6 eV), and Cu(OH)<sub>2</sub> (935.4 and 954.3 eV), indicating that Cu was significantly oxidized during the postannealing process of the VO<sub>x</sub> layer.<sup>34</sup> Hence, it can be concluded that graphene acts as a barrier for interdiffusion (Figure 4b) between Cu and VO<sub>x</sub>, protecting the underlying Cu substrate from oxidation and the top VO<sub>x</sub> layer from contamination, as illustrated in the inset of Figure 4c.

To identify the thermochromic properties of the graphene-supported VO<sub>2</sub> (VO<sub>2</sub>/graphene) films, we measured temperature-dependent optical transmittance of the films (Figure 5). A VO<sub>2</sub>/graphene film shows an optical transparency of 65.4% at the 550 nm wavelength and displays a typical thermochromic behavior with an abrupt change in the infrared region when the transmittance of the film was measured at 25 and 100 °C (Figure 5b).

The temperature-dependent optical transmission (at the wavelength of 2500 nm) and thermal hysteresis loop of VO<sub>2</sub>/graphene/PET film are shown in Figure 5c. Through heating and cooling cycles, the VO<sub>2</sub>/graphene/PET film undergoes a reversible phase transition with a NIR switching efficiency of  $\Delta T_r = 53\%$  at  $\lambda = 2500$  nm and shows the characteristic hysteric

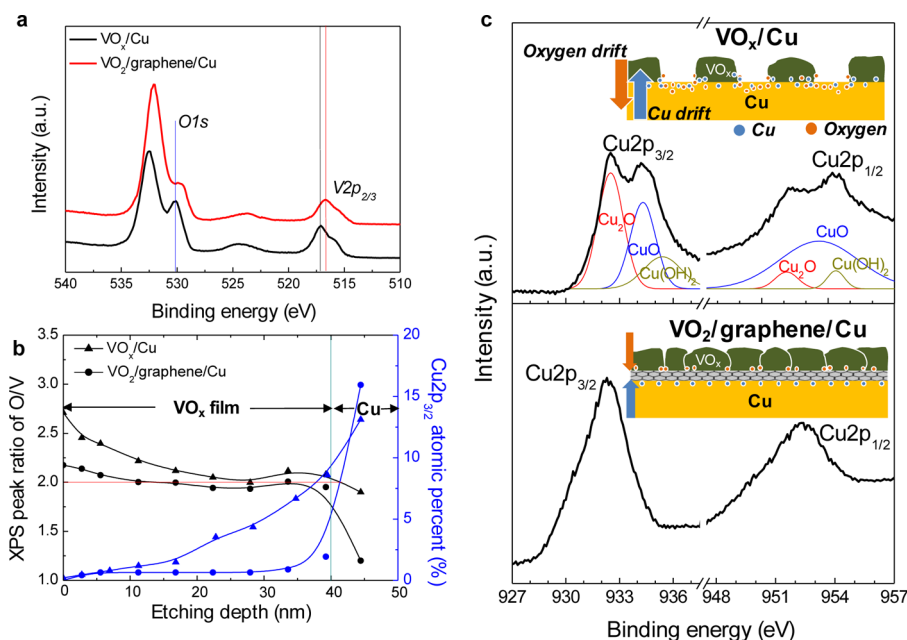


**Figure 4.** X-ray photoelectron spectroscopy (XPS) spectra of the graphene-supported  $\text{VO}_2$ . (a) XPS spectra of the graphene-supported  $\text{VO}_2$  ( $\text{VO}_2/\text{graphene}/\text{Cu}$ ) and the graphene-free  $\text{VO}_x$  films ( $\text{VO}_x/\text{Cu}$ ). (b) XPS depth profile showing the variation in the O/V peak ratio and the migration of copper contaminant. (c) XPS core-level  $\text{Cu}2p$  spectra of  $\text{VO}_x/\text{Cu}$  (top panel) and  $\text{VO}_2/\text{graphene}/\text{Cu}$  (bottom panel).

behavior with  $\Delta T = 9.8$  °C. While the hysteresis is relevant to the multidomain  $\text{VO}_2$  structure, nanosized  $\text{VO}_2$  crystals, and other parameters,<sup>14,35,36</sup> a relatively large hysteresis observed for  $\text{VO}_2/\text{graphene}/\text{PET}$  film is partially attributed to the presence of other  $\text{VO}_x$  phases such as  $\text{V}_2\text{O}_5$  and  $\text{V}_3\text{O}_5$ .<sup>37,38,41</sup> Graphene-supported  $\text{VO}_2$  shows two distinct transition temperatures of 65.4 °C on heating and 56.6 °C on cooling, giving the transition temperature  $T_c = 61$  °C from  $T_c = (T_{\text{heating}} + T_{\text{cooling}})/2$ . This indicates that graphene-supported  $\text{VO}_2$  showed a transition temperature lower than those measured for stoichiometric  $\text{VO}_2$  single crystals.<sup>1–6,14</sup> In general, depression of the phase transition in  $\text{VO}_2$  can have several origins: doping with other transition metals, strain, structural ordering, and scaling to nanoscale dimensions.<sup>13–15,39–41</sup> As the  $\text{VO}_2$  preparation method described here does not use any other transition metals, we attribute depression of the phase transition temperature to the effect of graphene support on reducing  $\text{VO}_2$  crystal size to nanoscale. In addition, with the high thermal conductivity reported for the graphene, the efficient heat transfer from graphene to  $\text{VO}_2$  may account for the depression of MIT temperature. Further work is underway to further understand the effect of underlying graphene on the phase transition characteristics of the graphene-supported  $\text{VO}_2$ .

We also evaluated the bending stability of the  $\text{VO}_2/\text{graphene}/\text{PET}$  film by measuring resistance change ( $\Delta R/R_0$ ) as a function of strain (inset of Figure 5d). A minimal resistance change over a strain ranging from 1 to 6% suggests that graphene-supported  $\text{VO}_2$  film is mechanically flexible without any serious mechanical damage or fracture of the film.<sup>25,42</sup> It is noted that we

measured the resistance of the  $\text{VO}_2/\text{graphene}$  hybrid film upon bending, and the measured values reflect the combined resistance of  $\text{VO}_2$  and graphene layers. For the repetitive bending cycling test, the flexible  $\text{VO}_2/\text{graphene}/\text{PET}$  film was tested on an automated bending machine. As shown in Figure 5d, the  $\Delta R/R_0$  values of the film were maintained when bent over 1000 times, indicating an excellent flexibility of the film. These results also suggest that there were no significant changes in the structure of graphene-supported  $\text{VO}_2$  films and the adhesion at the interface between graphene support and  $\text{VO}_2$  crystals.

The above results suggest that the graphene-supported  $\text{VO}_2$  film can be readily applicable to a new type of energy-efficient flexible film that automatically limits the optical transmission when the temperature reaches a defined value. As a prototype, we fabricated a model house with  $\text{VO}_2/\text{graphene}/\text{PET}$  thermochromic windows (Figure 5a) and evaluated its performance by measuring inner-house temperature changes after irradiation under an artificial solar lamp (Figure 5e)<sup>43</sup> (Supporting Information, Figure S6). As a control experiment, a window based on  $\text{VO}_2$ -free graphene/ $\text{PET}$  film was also tested. In the first 5 min of solar irradiation, the temperature is below the transition temperature of  $\text{VO}_2$ , and thus solar irradiation can be transmitted by the two windows, giving almost the same inner-house temperature. However, as the  $\text{VO}_2$  reached the transition temperature, the temperature difference between the two inner rooms was about 5.8 °C, indicating that a significant amount of irradiation was blocked by the graphene/ $\text{VO}_2$  window.

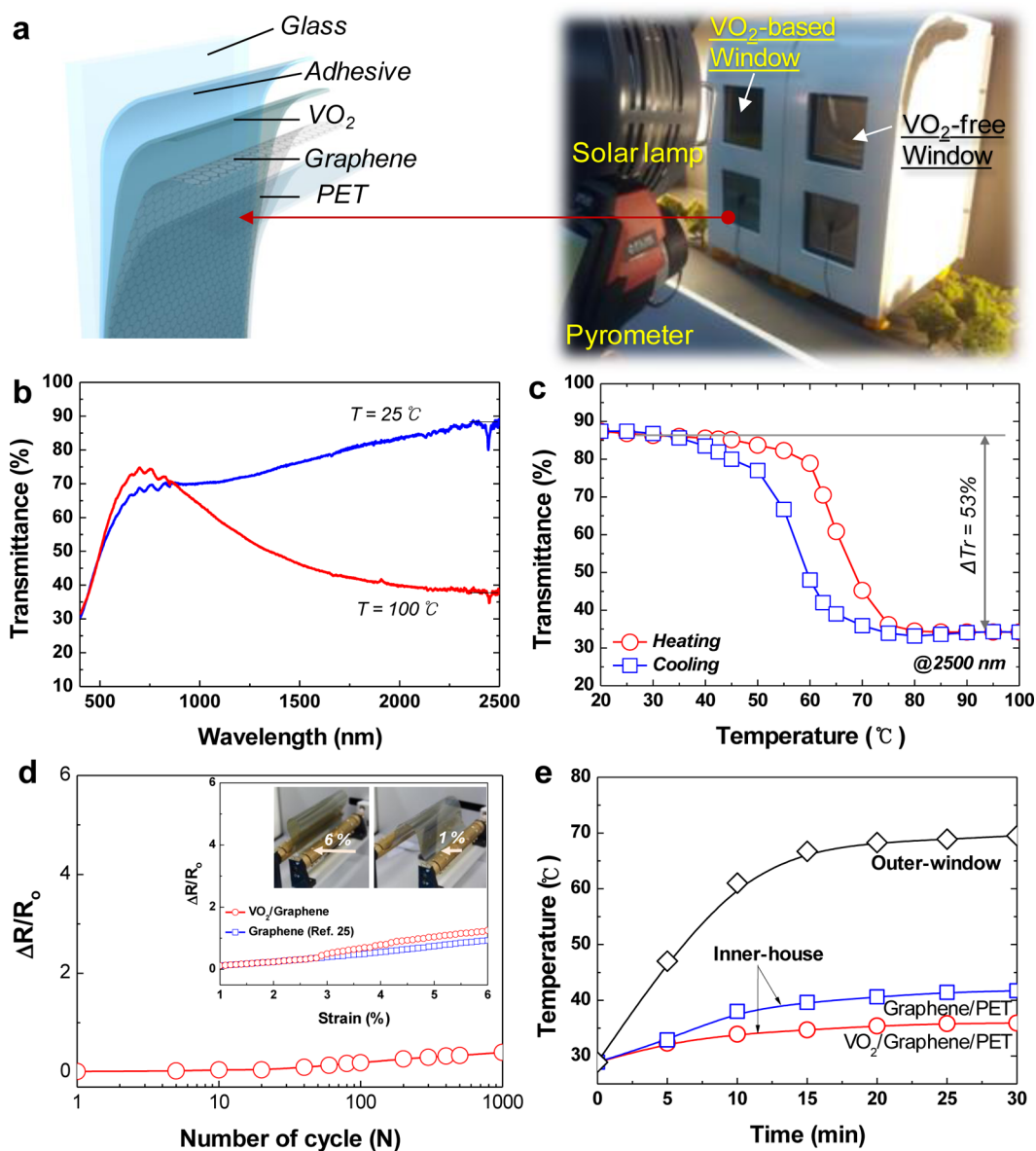


**Figure 5.** Thermochromic properties of the graphene-supported VO<sub>2</sub> film. (a) Structure of the graphene-supported VO<sub>2</sub> film. Photograph of model house equipped with VO<sub>2</sub>-based window (VO<sub>2</sub>/graphene/PET film) and VO<sub>2</sub>-free window (graphene/PET film). (b) Transmission spectra of the VO<sub>2</sub>/graphene/PET film taken at temperatures of 25 and 100 °C. (c) Temperature-dependent optical transmission (at λ = 2500 nm) of VO<sub>2</sub>/graphene/PET film. (d) Resistance change of a VO<sub>2</sub>/graphene/PET film against repeated bending cycle. The inset shows resistance changes as a function of strain. (e) Temperature change of model house upon solar irradiation as a function of exposure time.

## CONCLUSION

We present a fabrication method of mechanically flexible VO<sub>2</sub>-based thermo-chromic films. Graphene was employed to provide an atomically thin two-dimensional support for the growth of high-quality VO<sub>2</sub> and function as a shuttle to transfer the VO<sub>2</sub> layer to a flexible substrate. Large-area graphene-supported VO<sub>2</sub> films exhibited

mechanical flexibility while preserving its characteristic phase transition behavior with efficient switching behavior and lowered phase transition temperatures. The fabricated VO<sub>2</sub>/graphene hybrid films were integrated into the model house and shown to reduce the in-house temperature efficiently, demonstrating its potential as energy-saving smart window films.

## METHODS

**Preparation of Graphene-Supported VO<sub>2</sub> Films.** Single-layer graphene was grown on copper foils using a CVD method. First, the Cu foil (99.8%, Alfa-Aesar, item no. 13382) was loaded into a

quartz tube of the CVD system and annealed at 1000 °C under 90 mTorr with flowing 10 sccm of H<sub>2</sub> for 60 min to enlarge the single-crystalline graphene size of the Cu foil. The growth was initiated by flowing reaction gas mixtures (CH<sub>4</sub>/H<sub>2</sub> = 15:10 sccm)

under 560 mTorr for 25 min, followed by rapidly cooling the sample to room temperature ( $10\text{ }^{\circ}\text{C min}^{-1}$ ) with flowing  $\text{H}_2$  under 90 mTorr.<sup>25,26</sup>

The  $\text{VO}_x$  thin layer was prepared on the graphene/Cu and bare Cu substrates in a RF magnetron sputtering system. Sputtering was carried out with a water-cooled vanadium metal target (100 mm diameter, purity 99.99%). Prior to the deposition of  $\text{VO}_x$ , the substrate was presputtered by Ar ion plasma to eliminate contamination. Deposition was carried out at room temperature under argon (97 sccm) and oxygen (3 sccm) flowing for 40 min, and RF power of 300 W and a total pressure of 0.63 Pa were maintained during the deposition. For  $\text{VO}_2$  single-phase formation, postannealing of  $\text{VO}_x$  thin film on the graphene/Cu substrate was performed at  $500\text{ }^{\circ}\text{C}$  for 30 min under high vacuum of  $\sim 10^{-5}$  Pa with 50 sccm flowing  $\text{O}_2$ .

For the transfer of the film onto the PET substrate, the as-produced  $\text{VO}_2$ /graphene/Cu film was attached to a thermal release tape (Nitto Denko) by applying a pressure of  $\sim 0.2$  MPa using a roller. After etching the Cu layer and rinsing the residual etchant using deionized water, the  $\text{VO}_2$ /graphene on thermal release tape was laminated with PET film and exposed to mild heat ( $120\text{ }^{\circ}\text{C}$ ). Some of the  $\text{VO}_2$ /graphene/Cu film sample was coated with a thin layer of poly(methylmethacrylate) (PMMA), and then the underlying Cu foil was etched away in aqueous 0.1 M ammonium persulfate solution. After several washes with deionized water, the PMMA-backed  $\text{VO}_2$ /graphene was transferred onto  $\text{SiO}_2$  (300 nm)/Si substrates.<sup>25</sup>

**Characterization.** Morphologies of the  $\text{VO}_2$  film were examined by field-emission scanning electron microscope (FE-SEM, JSM-6490) and transmission electron microscopy (TEM, JEM-2100F operated at 200 kV). Phase identification was performed using X-ray diffraction (XRD, Bruker D8 Advance with  $\text{Cu K}\alpha$  radiation,  $\lambda = 1.54056\text{ \AA}$ ). Raman spectrum was obtained using the Renishaw inVia Raman microscope spectrometer with 514 nm wavelength excitation. X-ray photoelectron spectroscopy (XPS, Sigma Probe ThermoVG) was performed using monochromatic Al  $\text{K}\alpha$  radiation. Thermochromic switching characteristics were monitored on a UV-vis-NIR spectrophotometer (JASCO V-670) equipped with a film heating unit in the wavelength range of 300–2500 nm. The temperature was measured using a thermocouple in contact with films and was controlled through a temperature-controlling unit. Hysteresis loop was measured by collecting transmittance of films at a fixed wavelength (2500 nm) at a temperature interval of  $9.8\text{ }^{\circ}\text{C}$ . A model house ( $25 \times 20 \times 30\text{ cm}^3$ ) was made of boards measuring 10 mm in thickness, and  $\text{VO}_2$ /graphene/PET film was attached to the front windows ( $12 \times 12\text{ cm}^2$ ). An artificial solar lamp was used as the heat source to simulate solar radiation and positioned at a distance of 40 cm from the smart window.<sup>43</sup> Pyrometer was used to measure the temperature of the window, and two thermocouples were installed inside each house to monitor inner-house temperatures.

**Conflict of Interest:** The authors declare no competing financial interest.

**Acknowledgment.** This work was supported by Technology Innovation Program (No. 10044410, Commercialization of flexible touch panels based on  $900 \times 1600\text{ mm}^2$  large, less than 1 nm thick graphene film synthesis technique) funded by the Ministry of Trade, Industry and Energy, Energy Efficiency & Resources of the Korea Institute of Energy Technology Evaluation and Planning (KETEP) (No. 2012T100201723) funded by the Korea government Ministry of Knowledge Economy, Priority Research Centers Program (GT-SWS-11-01-004-0, Global Top Project; The Eco-Innovation Project) funded by Korea Ministry of Environment, the Global Frontier Research Program through the National Research Foundation (NRF) (No. 2011-0031630, from the Center for Advanced Soft Electronics) funded by the Ministry of Education, Science and Technology (MEST) of Korea, and K.S.K. was supported by Priority Research Centers Program (2010-0020207) through the NRF funded by the Ministry of Education, Basic Science Program (2011-0029645), Nano Material Technology Development Program through the NRF funded by the Ministry of Science, ICT and Future Planning (2012M3A7B4049888) and TJ Park Science Fellowship of POSCO

TJ Park Foundation. TEM studies were performed at UNIST Central Research Facilities (UCRF) at UNIST, and we thank Prof. S.M. Ryu (Kyung Hee U.) and Prof. E.J. Choi (The U. of Seoul) for helpful comments.

**Supporting Information Available:** Experimental methods and additional results. This material is available free of charge via the Internet at <http://pubs.acs.org>.

## REFERENCES AND NOTES

- Morin, F. J. Oxides Which Show a Metal-to-Insulator Transition at the Neel Temperature. *Phys. Rev. Lett.* **1959**, *3*, 34–36.
- Wentzcovitch, R. M.; Schulz, W. W.; Allen, P. B.  $\text{VO}_2$ : Peierls or Mott-Hubbard? View from Band Theory. *Phys. Rev. Lett.* **1994**, *72*, 3389–3392.
- Cavalleri, A.; Dekorsy, T.; Chong, H. H. W.; Kieffer, J. C.; Schoenlein, R. W. Evidence for a Structurally-Driven Insulator-to-Metal Transition in  $\text{VO}_2$ : A View from the Ultrafast Timescale. *Phys. Rev. B* **2004**, *70*, 161102.
- Kim, T.-H.; Angst, M.; Hu, B.; Jin, R.; Zhang, X.-G.; Wendelken, J. F.; Plummer, E. W.; Li, A.-P. Imaging and Manipulation of the Competing Electronic Phases near the Mott Metal-Insulator Transition. *Proc. Natl. Acad. Sci. U.S.A.* **2010**, *107*, 5272–5275.
- Wu, C.; Wei, H.; Ning, B.; Xie, Y. New Vanadium Oxide Nanostructures: Controlled Synthesis and Their Smart Electrical Switching Properties. *Adv. Mater.* **2010**, *22*, 1972–1976.
- Wu, J.; Gu, Q.; Guiton, B. S.; de Leon, N. P.; Ouyang, L.; Park, H. Strain-Induced Self Organization of Metal-Insulator Domains in Single-Crystalline  $\text{VO}_2$  Nanobeams. *Nano Lett.* **2006**, *6*, 2313–2317.
- Qazilbash, M. M.; Brehm, M.; Chae, B.-G.; Ho, P.-C.; Andreev, G. O.; Kim, B.-J.; Yun, S. J.; Balatsky, A. V.; Maple, M. B.; Keilmann, F.; *et al.* Mott Transition in  $\text{VO}_2$  Revealed by Infrared Spectroscopy and Nano-Imaging. *Science* **2007**, *318*, 1750–1753.
- Kübler, C.; Ehrke, H.; Huber, R.; Lopez, R.; Halabica, A.; Haglund, R. F., Jr.; Leitenstorfer, A. Coherent Structural Dynamics and Electronic Correlations during an Ultrafast Insulator-to-Metal Phase Transition in  $\text{VO}_2$ . *Phys. Rev. Lett.* **2007**, *99*, 116401.
- Strelcov, E.; Lilach, Y.; Kolmakov, A. Gas Sensor Based on Metal-Insulator Transition in  $\text{VO}_2$  Nanowire Thermistor. *Nano Lett.* **2009**, *9*, 2322–2326.
- Appavoo, K.; Haglund, R. F., Jr. Detecting Nanoscale Size Dependence in  $\text{VO}_2$  Phase Transition Using a Split-Ring Resonator Metamaterial. *Nano Lett.* **2011**, *11*, 1025–1031.
- Kim, D. H.; Kwok, H. S. Pulsed Laser Deposition of  $\text{VO}_2$  Thin Films. *Appl. Phys. Lett.* **1994**, *65*, 3188–3190.
- Gea, L. A.; Boatner, L. A. Optical Switching of Coherent  $\text{VO}_2$  Precipitates Formed in Sapphire by Ion Implantation and Annealing. *Appl. Phys. Lett.* **1996**, *68*, 3081–3083.
- Manning, T. D.; Parkin, I. P.; Pemble, M.; Sheel, D.; Vernardou, D. Intelligent Window Coatings: Atmospheric Pressure Chemical Vapor Deposition of Tungsten-Doped Vanadium Dioxide. *Chem. Mater.* **2004**, *16*, 744–749.
- Parkin, I. P.; Manning, T. D. Intelligent Thermochromic Windows. *J. Chem. Educ.* **2006**, *83*, 393–400.
- Gao, Y.; Luo, H.; Zhang, Z.; Kang, L.; Chen, Z.; Du, J.; Kanehira, M.; Cao, C. Nanoceramic  $\text{VO}_2$  Thermochromic Smart Glass: A Review on Progress in Solution Processing. *Nano Energy* **2012**, *1*, 221–246.
- Gao, Y.; Wang, S.; Kang, L.; Chen, Z.; Du, J.; Liu, X.; Luo, H.; Kanehira, M.  $\text{VO}_2$ -Sb:SnO<sub>2</sub> Composite Thermochromic Smart Glass Foil Energy. *Energy Environ. Sci.* **2012**, *5*, 8234–8237.
- Chae, B.-G.; Kim, H.-T.; Yun, S.-J.; Kim, B.-J.; Lee, Y.-W.; Kang, K.-Y. Comparative Analysis of  $\text{VO}_2$  Thin Films Prepared on Sapphire and  $\text{SiO}_2$ /Si Substrates by the Sol-Gel Process. *Jpn. J. Appl. Phys.* **2007**, *46*, 738–743.
- Li, S.-Y.; Niklasson, G. A.; Granqvist, C. G. Thermochromic Fenestration with  $\text{VO}_2$ -Based Materials: Three Challenges and How They Can Be Met. *Thin Solid Films* **2012**, *520*, 3823–3828.
- Chae, B. G.; Kim, H. T.; Yun, S. J. Characteristics of W- and Ti-Doped  $\text{VO}_2$  Thin Films Prepared by Sol-Gel Method. *Electrochem. Solid Lett.* **2008**, *11*, D53–D55.

20. Chae, B. G.; Kim, H. T. Effects of W Doping on the Metal–Insulator Transition in Vanadium Dioxide Film. *Physica B* **2010**, *405*, 663–667.
21. Takahashi, I.; Hibino, M.; Kudo, T. Thermochromic  $V_{1-x}W_xO_2$  Thin Films Prepared by Wet Coating Using Polyvanadate Solutions. *Jpn. J. Appl. Phys.* **1996**, *35*, L438–L440.
22. Geim, A. K.; Novoselov, K. S. The Rise of Graphene. *Nat. Mater.* **2007**, *6*, 183–191.
23. Lee, C.; Wei, X.; Kysar, J. W.; Hone, J. Measurement of the Elastic Properties and Intrinsic Strength of Monolayer Graphene. *Science* **2008**, *321*, 385–388.
24. Nair, R. R.; Blake, P.; Grigorenko, A. N.; Novoselov, K. S.; Booth, T. J.; Stauber, T.; Peres, N. M. R.; Geim, A. K. Fine Structure Constant Defines Visual Transparency of Graphene. *Science* **2008**, *320*, 1308.
25. Bae, S.; Kim, H.; Lee, Y.; Xu, X.; Park, J.-S.; Zheng, Y.; Balakrishnan, J.; Lei, T.; Kim, H. R.; Song, Y. I.; et al. Roll-to-Roll Production of 30-Inch Graphene Films for Transparent Electrodes. *Nat. Nanotechnol.* **2010**, *5*, 574–578.
26. Kang, J.; Hwang, S.; Kim, J. H.; Kim, M. H.; Ryu, J.; Seo, S. J.; Hong, B. H.; Kim, M. K.; Choi, J.-B. Efficient Transfer of Large-Area Graphene Films onto Rigid Substrates by Hot Pressing. *ACS Nano* **2012**, *6*, 5360–5365.
27. Li, X.; Cai, W.; An, J.; Kim, S.; Nah, J.; Yang, D.; Piner, R.; Velamakanni, A.; Jung, I.; Tutuc, E.; et al. Large-Area Synthesis of High-Quality and Uniform Graphene Films on Copper Foils. *Science* **2009**, *324*, 1312–1314.
28. Kim, Y.-J.; Yoo, H.; Lee, C.-H.; Park, J. B.; Baek, H.; Kim, M.; Yi, G.-C. Position- and Morphology-Controlled ZnO Nanostructures Grown on Graphene Layers. *Adv. Mater.* **2012**, *24*, 5565–5569.
29. Ferrari, A. C.; Meyer, J. C.; Scardaci, V.; Casiraghi, C.; Lazzeri, M.; Mauri, F.; Piscanec, S.; Jiang, D.; Novoselov, K. S.; Roth, S.; et al. Raman Spectrum of Graphene and Graphene Layers. *Phys. Rev. Lett.* **2006**, *97*, 187401.
30. Ryu, S.; Liu, L.; Berciaud, S.; Yu, Y.-J.; Liu, H.; Kim, P.; Flynn, G. W.; Brus, L. E. Atmospheric Oxygen Binding and Hole Doping in Deformed Graphene on a  $SiO_2$  Substrate. *Nano Lett.* **2010**, *10*, 4944–4951.
31. Jones, A. C.; Berweger, S.; Wei, J.; Cobden, D.; Raschke, M. B. Nano-optical Investigations of the Metal-Insulator Phase Behavior of Individual  $VO_2$  Microcrystals. *Nano Lett.* **2010**, *10*, 1574–1581.
32. Kim, B.-J.; Lee, Y. W.; Chae, B.-G.; Yun, S. J.; Oh, S.-Y.; Kim, H.-T.; Lim, Y.-S. Temperature Dependence of the First-Order Metal-Insulator Transition in  $VO_2$  and Programmable Critical Temperature Sensor. *Appl. Phys. Lett.* **2007**, *90*, 023515.
33. Yang, Z.; Ramanathan, S. Direct Measurement of Compositional Complexity-Induced Electronic Inhomogeneity in  $VO_2$  Thin Films Grown on Gate Dielectrics. *Appl. Phys. Lett.* **2011**, *98*, 192113.
34. Chen, S.; Brown, L.; Levendorf, M.; Cai, W.; Ju, S.-Y.; Edgeworth, J.; Li, X.; Magnuson, C. W.; Velamakanni, A.; Piner, R. D.; et al. Oxidation Resistance of Graphene-Coated Cu and Cu/Ni Alloy. *ACS Nano* **2011**, *5*, 1321–1327.
35. Zhang, Z.; Gao, Y.; Luo, H.; Kang, L.; Chen, Z.; Du, J.; Kanehira, M.; Zhang, Y.; Wang, Z. L. Solution-Based Fabrication of Vanadium Dioxide on F:SnO<sub>2</sub> Substrates with Largely Enhanced Thermochromism and Low-Emissivity for Energy-Saving Applications. *Energy Environ. Sci.* **2011**, *4*, 4290–4297.
36. Xu, G.; Huang, C.-M.; Tazawa, M.; Jin, P.; Chen, D.-M.; Miao, L. Electron Injection Assisted Phase Transition in a Nano-Au- $VO_2$  Junction. *Appl. Phys. Lett.* **2008**, *93*, 061911.
37. Eiji, K.; Jeremy, A. T. Effects of Microstructures and Non-stoichiometry on Electrical Properties of Vanadium Dioxide Films. *J. Vac. Sci. Technol., A* **1989**, *7*, 1314–1317.
38. Zheng, Y.; Shriram, R. Direct Measurement of Compositional Complexity-Induced Electronic Inhomogeneity in  $VO_2$  Thin Films Grown on Gate Dielectrics. *Appl. Phys. Lett.* **2011**, *98*, 192113.
39. Gao, Y.; Wang, S.; Luo, H.; Dai, L.; Cao, C.; Liu, Y.; Chen, Z.; Kanehira, M. Enhanced Chemical Stability of  $VO_2$  Nanoparticles by the Formation of  $SiO_2/VO_2$  Core/Shell Structures and the Application to Transparent and Flexible  $VO_2$ -Based Composite Foils with Excellent Thermochromic Properties for Solar Heat Control. *Energy Environ. Sci.* **2012**, *5*, 6104–6110.
40. Gao, Y.; Cao, C.; Dai, L.; Luo, H.; Kanehira, M.; Ding, Y.; Wang, Z. L. Phase and Shape Controlled  $VO_2$  Nanostructures by Antimony Doping. *Energy Environ. Sci.* **2012**, *5*, 8708–8715.
41. Kim, H.; Kim, Y.; Kim, T. Y.; Jang, A.-R.; Jeong, H. Y.; Han, S. H.; Yoon, D. H.; Shin, H. S.; Bae, D. J.; Kim, K. S.; et al. Enhanced Optical Response of Hybridized  $VO_2$ /Graphene Films. *Nanoscale* **2013**, *5*, 2632–2636.
42. Lee, C.-H.; Kim, Y.-J.; Hong, Y. J.; Jeon, S.-R.; Bae, S.; Hong, B. H.; Yi, G.-C. Flexible Inorganic Nanostructure Light-Emitting Diodes Fabricated on Graphene Films. *Adv. Mater.* **2011**, *23*, 4614–4619.
43. Sato, T.; Sato, I. Requirement Governing Light Sources Used for Color Evaluation. *Proceedings of the 8th Congress of the International Colour Association*; Kyoto, Japan, May 25–30, 1997; Vol. 1, pp 415–418.